



HAL
open science

Persistent Influence of Non-Dipole Geomagnetic Field on East Asia Over the Past 4,000 Years

Hai Li, Jianhui Tang, Congcong Gai, Weijie Zhang, Fabien Humbert,
Youzhong Ni, Yu-min Chou, Qingsong Liu

► **To cite this version:**

Hai Li, Jianhui Tang, Congcong Gai, Weijie Zhang, Fabien Humbert, et al.. Persistent Influence of Non-Dipole Geomagnetic Field on East Asia Over the Past 4,000 Years. *Journal of Geophysical Research: Solid Earth*, 2023, 128 (12), 10.1029/2023JB027359 . hal-04774764

HAL Id: hal-04774764





<https://hal.science/hal-04774764v1>

Submitted on 8 Nov 2024

HAL is a multi-disciplinary open access archive for the deposit and dissemination of scientific research documents, whether they are published or not. The documents may come from teaching and research institutions in France or abroad, or from public or private research centers.

L'archive ouverte pluridisciplinaire **HAL**, est destinée au dépôt et à la diffusion de documents scientifiques de niveau recherche, publiés ou non, émanant des établissements d'enseignement et de recherche français ou étrangers, des laboratoires publics ou privés.

Persistent Influence of Non-Dipole Geomagnetic Field on East Asia Over the Past 4,000 Years

Hai Li¹ , Jianhui Tang² , Congcong Gai¹, Weijie Zhang¹, Fabien Humbert^{1,3}, Youzhong Ni⁴, Yu-Min Chou^{1,5} , and Qingsong Liu^{1,5,6} 

¹Centre for Marine Magnetism (CM2), Department of Ocean Science and Engineering, Southern University of Science and Technology, Shenzhen, China, ²Key Laboratory of Coastal Environmental Processes and Ecological Remediation, Yantai Institute of Coastal Zone Research, Chinese Academy of Sciences, Yantai, China, ³Laboratoire Géosciences et Environnement Cergy (GEC), CY Cergy Paris Université, Neuville sur Oise, France, ⁴Sheshan Earthquake Monitoring Center Station of Shanghai Seismological Bureau, Shanghai, China, ⁵Southern Marine Science and Engineering Guangdong Laboratory (Guangzhou), Guangzhou, China, ⁶Shanghai Sheshan National Geophysical Observatory, Shanghai, China

Key Points:

- A multi-decadal resolution paleomagnetic record spanning approximately 4,000 years has been derived from sediments in the Bohai Sea, China
- The paleomagnetic behavior differs between middle and low latitudes across East Asia, indicating the variation of the Siberian flux lobe
- The disparity in inclination between the Chinese and Levantine spikes implies that these spikes arise from separate magnetic flux patches

Supporting Information:

Supporting Information may be found in the online version of this article.

Correspondence to:

Y.-M. Chou and Q. Liu,
chouym@sustech.edu.cn;
qslu@sustech.edu.cn

Citation:

Li, H., Tang, J., Gai, C., Zhang, W., Humbert, F., Ni, Y., et al. (2023). Persistent influence of non-dipole geomagnetic field on East Asia over the past 4,000 years. *Journal of Geophysical Research: Solid Earth*, 128, e2023JB027359. <https://doi.org/10.1029/2023JB027359>

Received 29 JUN 2023

Accepted 9 DEC 2023

Author Contributions:

Formal analysis: Yu-Min Chou, Qingsong Liu

Investigation: Hai Li

Methodology: Congcong Gai, Weijie Zhang, Fabien Humbert, Youzhong Ni, Yu-Min Chou, Qingsong Liu

Resources: Youzhong Ni, Yu-Min Chou

Supervision: Yu-Min Chou, Qingsong Liu

Writing – original draft: Hai Li

Writing – review & editing: Jianhui Tang, Congcong Gai, Weijie Zhang, Fabien Humbert, Youzhong Ni, Yu-Min Chou, Qingsong Liu

Abstract The observed variations in intense geomagnetic flux lobes have a significant impact on regional geomagnetic fields, and produce unique geomagnetic characteristics. To investigate the time-dependent effect of the Siberian flux lobe on the geomagnetic field in East Asia, we reconstructed a stacked full-vector paleomagnetic secular variation record (since 2000 BCE) from three sediment cores collected in the Bohai Sea, China. Age models of the studied cores were established through a combination of radiocarbon ¹⁴C dating and inter-profile correlation of mass-normalized magnetic susceptibility. Rock magnetic results indicate that fine-grained magnetite is the primary remanent carrier. We found that the paleomagnetic field records in the Bohai Sea correspond more closely with those from the middle latitudes, rather than the low latitudes. This was primarily attributed to the variation of the Siberian flux lobe. This study provides a better understanding of the contrasting patterns of regional geomagnetic fields in East Asia, and emphasizes the significant role played by the Siberian flux intensity lobe in shaping their formation.

Plain Language Summary The Earth's magnetic field is in a constant state of flux, both temporally and spatially, and plays a crucial role in protecting our planet from solar wind and cosmic rays. The long-term variation of the Earth's magnetic field is closely linked with the magnetic flux patch situated at the core-mantle boundary. However, our understanding of the evolution of magnetic flux patches has been limited by the use of short-term instrumental data and discrete archeomagnetic data. In this paper, we reconstruct a ~4,000-year high-resolution full-vector paleomagnetic record from sediments in the Bohai Sea, China. Our findings reveal a clear contrast in the paleomagnetic variations between the middle and low latitudes of East Asia. We proposed that the Siberian flux intensity lobe likely played an important role in the observed paleomagnetic behavior discrepancy between the low- and mid-latitudes of East Asia.

1. Introduction

The main geomagnetic field, originating from the Earth's outer core, can provide valuable insights into the geodynamo processes (e.g., Buffett, 2000; Tarduno et al., 2015). The present-day Earth's surface geomagnetic field is characterized by the high intensity lobes in Siberia and Canada, as well as a weak intensity anomaly located primarily in the South Atlantic Ocean and extending to South America and South Africa, known as the South Atlantic Anomaly (Alken et al., 2021; Finlay et al., 2020). These magnetic field characteristics may result from the magnetic flux patches of the radial field at the core mantle boundary (CMB) (Finlay et al., 2020; Livermore et al., 2020; Tarduno et al., 2015). Numerical magnetic field models show that magnetic flux patches on the CMB are not stationary (Amit et al., 2010, 2011). Instead, they may exhibit episodic behavior such as disappearing, reappearing, or drifting from one preferred location to another (Amit et al., 2010).

Recent research suggested that the magnetic flux lobes on the CMB under Canada and Siberia could affect the position and movement of the north magnetic pole and virtual geomagnetic pole (Caricchi et al., 2022; Livermore et al., 2020). The axial dipole moment of Earth's magnetic field appears to be related to the waxing and waning of the normal flux lobes in the Northern Hemisphere (Pavón-Carrasco et al., 2014) and the expansion and migration of reversed flux patches (RFPs) in the Southern Hemisphere (Metman et al., 2018). Additionally, magnetic

flux patches can trigger abrupt changes in geomagnetic fields, such as the Levantine Iron Age Anomaly (Osete et al., 2020).

Based on paleomagnetic secular variation (PSV) records, time-averaged geomagnetic field models over the past 7 ka (Bloxxham et al., 1989; Korte & Holme, 2010) and 10 ka (Constable et al., 2016) suggest that two magnetic flux lobes have long been existing in the Northern Hemisphere. The abnormal paleomagnetic features, such as shallow inclinations at 64–70 ka and a geomagnetic spike at ~12 ka in the subarctic and East Asia, suggest that the normal flux lobes may have persisted and influenced the high-latitude region magnetic field in the Northern Hemisphere over the past 140 ka (Zhong et al., 2020). Furthermore, the normal-polarity time-averaged field models over the past 5 million years, show two magnetic flux lobes beneath Siberia and Canada which are similar to the modern geomagnetic field (Johnson & Constable, 1995; Kelly & Gubbins, 1997), but in a weak and not necessarily robust way (Carlut & Courtillot, 1998; Khokhlov et al., 2006). However, the evolution and influences of such persistent magnetic flux lobes remain poorly constrained due to limited high-quality paleomagnetic records.

The Bohai Sea, located at the southeastern edge of the Siberian surface lobe (Figure 1a) resulting from the Siberian flux lobe (Bloxxham & Gubbins, 1985; Livermore et al., 2020), is a suitable area to investigate the characteristics and effects of the magnetic flux lobe. Moreover, relatively high sedimentation rates (>30 cm/ka) of the Bohai Sea provide an opportunity for reconstructing high-resolution paleoclimatic and paleomagnetic records (Yao et al., 2014). In this study, we derived high-resolution paleomagnetic records from three sediment cores in the Bohai Sea and discussed the potential influence of the Siberia flux lobe on the geomagnetic field in East Asia.

2. Background, Materials, and Methods

2.1. Regional Setting and Background

The Bohai Sea is a semi-closed inland sea that covers an area of ~78,000 km² and is connected to the Yellow Sea through the Bohai Strait (Figure 1b). The Sea is characterized by a maximum and average water depth of 84 and 18 m, respectively (M. Li et al., 2020). More than 30 rivers flow into the Bohai Sea, contributing a discharge of ~7.8 × 10⁸ tons of sediment annually, with the terrigenous input mainly from the Yellow, Haihe, Luanhe, and Liaohe Rivers. Regular semidiurnal tides govern most of the Bohai Sea, with certain locations also experiencing diurnal tides and irregular semidiurnal tides (Qiao et al., 2008). Ocean circulation within the Bohai Sea is primarily driven by the Yellow Sea Warm Current (YSWC) and Bohai Sea Coastal Current (Figure 1b).

2.2. Core Description and Sampling

Three piston cores, namely M12-8 (40.62°N, 121.36°E, 11 m depth, 3.2 m long), M5-8 (39.09°N, 120.0°E, 22 m depth, 3.46 m long), and BHB15-6 (38.55°N, 118.55°E, 20 m depth, 2.51 m long), were recovered from the Bohai Sea using a gravity piston corer (core diameter specification: 7 cm) during the cruise of North Yellow Sea-Bohai Sea Special Voyage in 2018 (Figure 1b), and all studied cores were not azimuthally orientated during coring. These cores predominantly consist of fine-grained sediments, such as gray clay and silty clay layers, with occasional intercalations of sand layers. We performed a continuous sampling along the central axis of each core segment using cubic plastic boxes (1.9 × 1.9 × 1.9 cm³) for paleomagnetic studies. 114, 129, and 159 samples were collected from cores BHB15-6, M12-8, and M5-8, respectively.

2.3. ¹⁴C Dating

¹⁴C dates were obtained using an accelerator mass spectrometry on bulk benthic foraminifera. The age models of the studied cores were estimated using the software *Undatable* (Lougheed & Obrochta, 2019) and the Marine20 calibration curve (Heaton et al., 2020). The *Undatable* setting parameters of *xfactor* = 0.1 and *bootpc* = 10 with a reservoir age of $\Delta R = -334 \pm 50$ years were based on Southon et al. (2002). Radiocarbon dates were measured at the Beta Analytic laboratory.

2.4. Magnetic Measurements

Anisotropy of magnetic susceptibility (AMS) and mass-normalized magnetic susceptibility (χ) were measured under a 200 A/m field at a frequency of 976 Hz. Temperature-dependence magnetic susceptibility (χ -*T*) curves

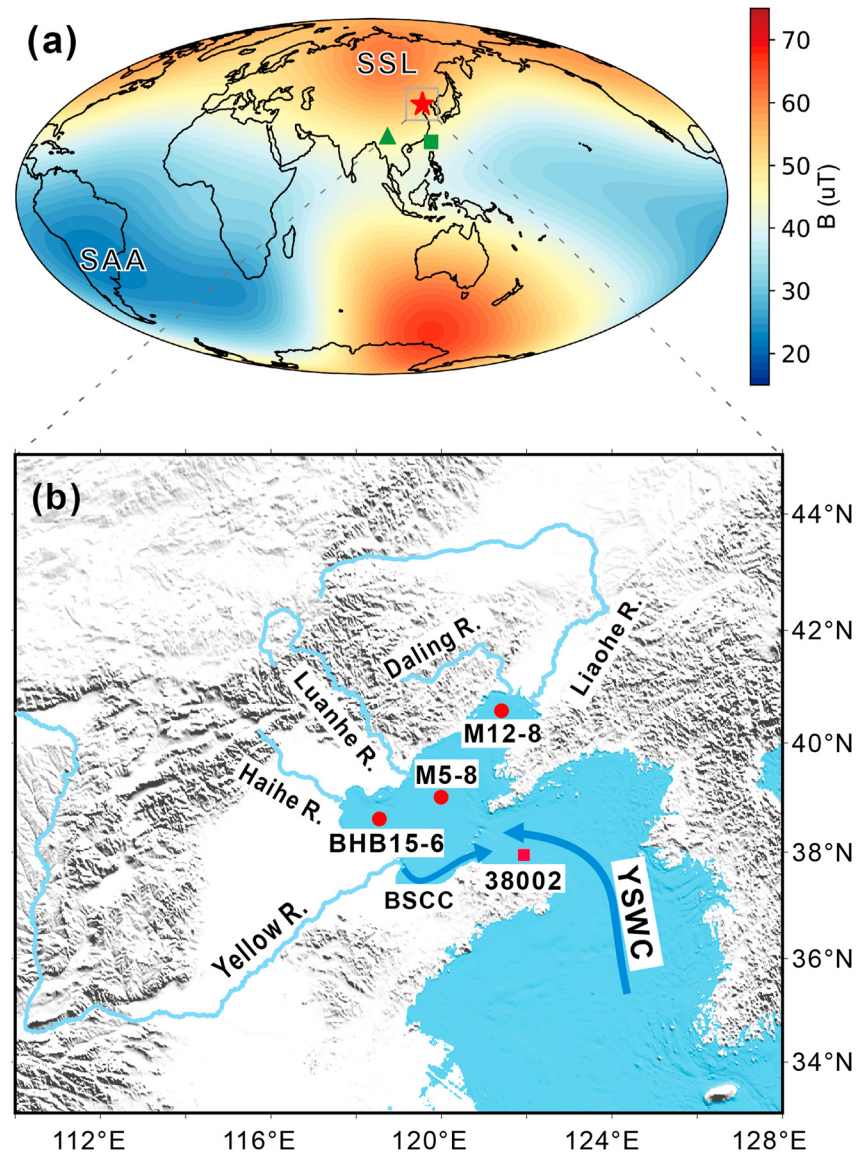


Figure 1. (a) Present-day magnetic field intensity at the Earth's surface, as calculated with the CALS10k.1b model (Korte et al., 2011). The red star indicates the Bohai Sea, the green triangle and square represent the location of Tengchong Qinghai Lake (Yang et al., 2022) and core OR1-715-21 (Huang et al., 2014), respectively. SSL: Siberian surface lobe, SAA: South Atlantic Anomaly. (b) Map of the Bohai Sea with locations of study cores and core 38002 (Y. Zhang et al., 2019; J. Zhang et al., 2020). YSWC: Yellow Sea Warm Current, BSCC: Bohai Sea Coastal Current.

for representative samples were measured in an argon atmosphere from room temperature to 700°C. χ , χ -T, and AMS were measured using an AGICO MFK2-FA system equipped with a CS-4 furnace, where χ -T was measured in an argon atmosphere.

Natural remanent magnetization (NRM) and anhysteretic remanent magnetization (ARM) were measured using a 2G Enterprises 755-4k U-Channel SQUID magnetometer. The NRM was measured and followed by stepwise alternating field (AF) demagnetization with 11 steps (0, 5, 10, 15, 20, 30, 40, 50, 65, 80, and 100 mT). Characteristic remanent magnetization (ChRM) was calculated by principal component analysis (Kirschvink, 1980). The ARM was imparted in a 0.05 mT DC bias field within a 100 mT AF peak field and then treated AF demagnetization in steps of 20, 30, 40, 50, 65, and 80 mT. The anhysteretic susceptibility (χ_{ARM}) was obtained in a 0.05 mT steady field. The relative paleointensity (RPI) was determined by calculating the slope of NRM versus ARM between AF demagnetization steps of 20 and 65 mT. Paleomagnetic measurements on discrete samples

were performed at the Environmental Magnetism laboratory of School of Earth Sciences, China University of Geosciences (Wuhan), China.

Isothermal remanent magnetizations (IRM) were imparted using a DPM1 digital pulse magnetizer and then measured with a JR-6 spinner magnetometer. IRM intensity acquired at 1 T field is defined as the saturation IRM (SIRM). A reversed field of 0.3 T was used to determine the S-ratio, which is defined as: $-IRM_{-0.3T}/SIRM$. Detailed IRM acquisition curves and first order reversal curves (FORC) measurements were performed using a Lake Shore 8600 Vibrating Sample Magnetometer. FORC was obtained with an averaging time of 0.1 s and a field step of 1.375 mT. FORC data were processed using the software FORCinel v. 3.0 with smoothing factors of $S_{c0} = 4$, $S_{c1} = 3.5$, $S_{b0} = 3.5$, and $S_{b1} = 3.5$ (Harrison & Feinberg, 2008). IRM acquisition curves were obtained by applying 100 nonlinear spaced field steps from 0.1 mT to 1 T. The IRM acquisition curves were decomposed using the software “pyIRM,” available at <https://github.com/botaoxiongyong/pyIRM> (Liu et al., 2019). All rock magnetic samples were measured at the Center for Marine Magnetism at Southern University of Science and Technology, Shenzhen, China.

3. Results

3.1. Age Models

Age-depth models for the studied cores were established by combining ^{14}C dates and correlating mass-normalized magnetic susceptibility curves among these cores (Figure 2). The radiocarbon dates for cores M12-8, M5-8, and BHB15-6 have been used to develop individual chronology by linear regression for these cores (Table S1 in Supporting Information S1). Magnetic analysis of Surface sediment from the Bohai Sea and surrounding rivers reveals that the Yellow River is the primary source of magnetic materials throughout the Bohai Sea (M. Li et al., 2020), while sediments from other rivers are deposited primarily in nearshore areas (Chen et al., 1982). These findings suggest that magnetic parameters, such as χ , can be used to refine the age model. Despite potential differences in the χ curves attributed to factors such as environmental processes, the correlating the χ variations among cores M12-8, M5-8, and BHB15-6 has indeed yielded several additional age tie points (Figure 2a). The age uncertainties for the χ correlation tie points were given by the initial age-depth model, which was established using ^{14}C dating and calculated using the *Undatable* software (Lougheed & Obrochta, 2019). The obtained age models for the sediment cores are shown in Figure 2b, with BHB15-6 covering the past 5.2 ka and M5-8 and M12-8 covering less than 2.8 ka. The averaged sedimentation rates of M12-8, M5-8, and BHB15-6 are approximately 140, 130, and 50 cm/ka, respectively. With a sampling interval of 2 cm, the theoretical temporal resolution ranges from about 15 to 40 years.

3.2. Rock Magnetic Results

The AMS results are displayed in Figure S1 in Supporting Information S1. The minimum susceptibility axes (k_{\min}) of most samples are nearly perpendicular to the horizontal plane (with a range of 70° and 90°), and the inclination of intermediate and maximum susceptibility axes (k_{int} and k_{\max}) tends to be horizontal, suggesting a typical normal depositional fabric (Hroudá & Kahan, 1991). The shallow k_{\min} ($<65^\circ$) of some sporadic samples may result from mechanical disturbances during sampling (T. Yang et al., 2019). Hence, these samples with shallow k_{\min} were not used to reconstruct the paleomagnetic records.

The χ - T heating curves of representative samples illustrate a unique Curie temperature at $\sim 580^\circ\text{C}$ (Figure 3c), which shows that magnetite is the primary magnetic carrier of the sediments (Dunlop & Özdemir, 1997). Above 600°C , a slight decline in χ in some χ - T heating curves (e.g., BHB15-6:193 cm) indicates the presence of hematite. The IRM acquisition curves for all samples were not saturated even at the field of 1 T, likely due to the existence of high-coercivity magnetic minerals (Figure 3a). The distribution of IRM acquisition curves can be fitted with three components for all samples (Figure 3b). Components 1 (green line, median field: ~ 11 – 22 mT, dispersion parameter: ~ 0.27 – 0.33) and component 2 (blue line, median field: ~ 40 – 52 mT, dispersion parameter: ~ 0.22 – 0.27) account for at least 85% of the total IRM, further suggesting that low-coercivity minerals are the predominant carrier of the remanent magnetization. In contrast, component 3 (orange line, 143 – 350 mT), representing the high-coercivity magnetic minerals such as hematite, has very low proportions.

FORC diagrams (Figure 4) of representative samples from the three studied cores displayed a clear ridge-like distribution along the B_c axis, which is commonly observed in samples with non-interacting single domain (SD) particles (Egli et al., 2010; Pike et al., 1999). Additionally, the FORC diagrams spreading along the B_u axis are a

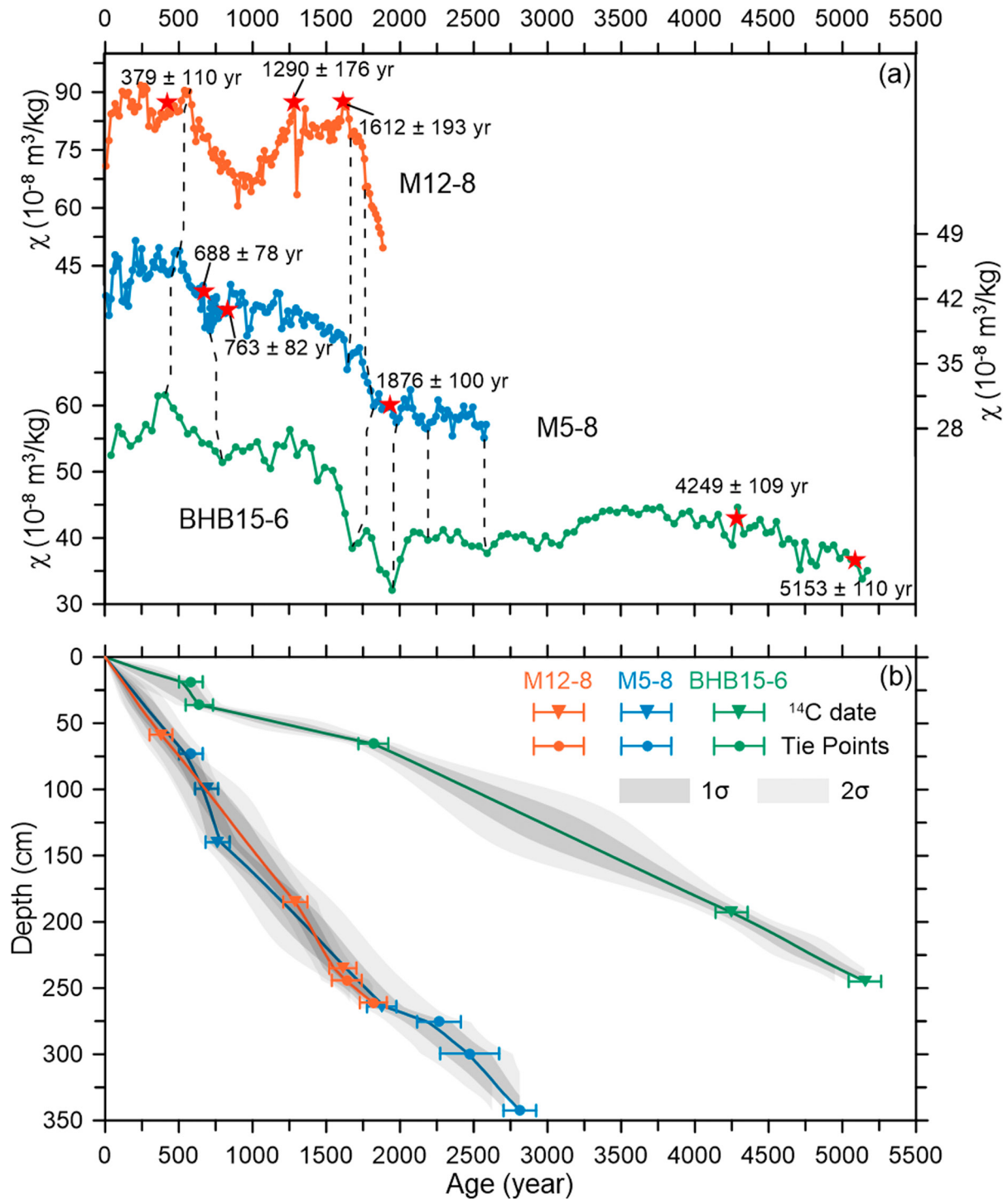


Figure 2. (a) Mass-normalized magnetic susceptibility (χ) of core M12-8, M5-8, and BHB15-6; the red stars indicated the ^{14}C dates which were calculated using the *Calib 8.2* software (Stuiver & Reimer, 1993) and the Marine20 calibration curve (Heaton et al., 2020). (b) Age-depth models for the studied cores were calculated using the *Undatable* software (Lougheed & Obrochta, 2019); tie points were derived from correlations among the magnetic susceptibility curves.

typical feature of the magnetic vortex state (Lascu et al., 2018; Roberts et al., 2017). Thus, the detrital ferromagnetic particles in the studied sediments are mainly composed of SD and vortex grains.

The S-ratio for cores M12-8 (~0.87–0.96, mean value: ~0.92), M5-8 (~0.82–0.94, mean value: ~0.86), and BHB15-6 (~0.84–0.94, mean value: ~0.87) indicate that low coercivity minerals are dominant (Figure S2 in

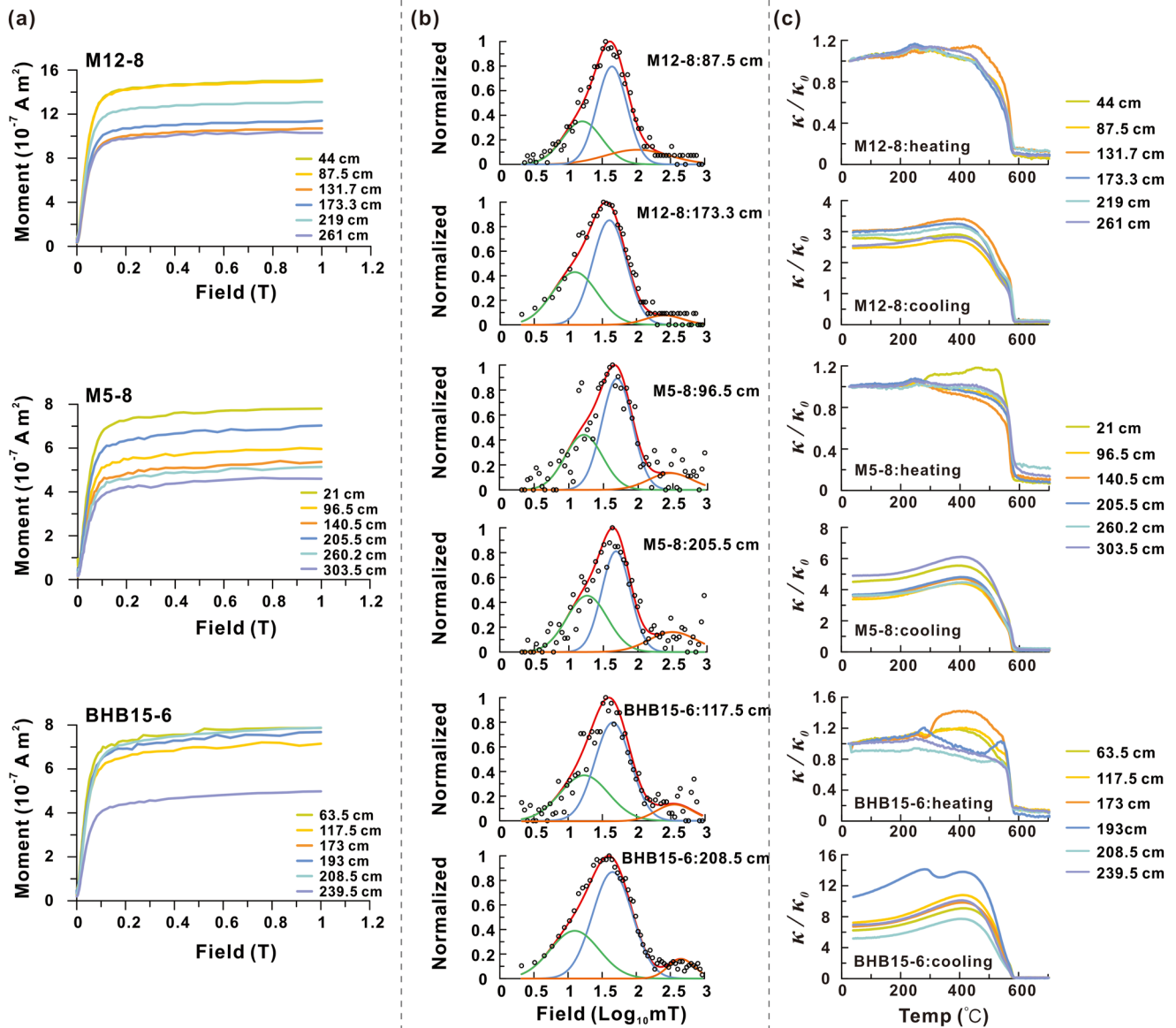


Figure 3. Rock magnetic properties of representative samples from cores M12-8, M5-8, and BHB15-6. (a) Isothermal remanent magnetization (IRM) acquisition curves. (b) IRM decomposition curves. The blue, green, orange, and red curves indicate components 1, 2, 3, and the fitted total spectrum, respectively; black circles represent the measured data. (c) χ -T curves, κ/κ_0 is the ratio of non-room over room temperature susceptibility.

Supporting Information S1). Additionally, values of the concentration-dependent magnetic parameters (i.e., χ , ARM, and SIRM) and relative magnetic grain size proxy (χ_{ARM}/χ) vary within a factor of 3, indicating a relative homogeneity in both the concentration (Tauxe, 1993) and grain size (J. King et al., 1982; J. W. King et al., 1983) of magnetic particles among all studied cores (Figure S2 in Supporting Information S1).

3.3. Demagnetization Results

NRM results of studied samples are generally completely demagnetized at around 100 mT (Figure S3 in Supporting Information S1). ChRM directions were generally estimated from AF steps between 20 and 65 mT. For most samples, maximum angular deviation values are lower than 6° (Figure 5d), indicating accurate ChRM results. The ChRM inclination data for each core mostly fall within the range of the normal polarity inclinations corresponding to the latitude of the site (Figure 5b, detailed in Figure S4 in Supporting Information S1). Declinations for all studied cores have been rotated to a mean of zero, under the assumption that each core spans sufficient time

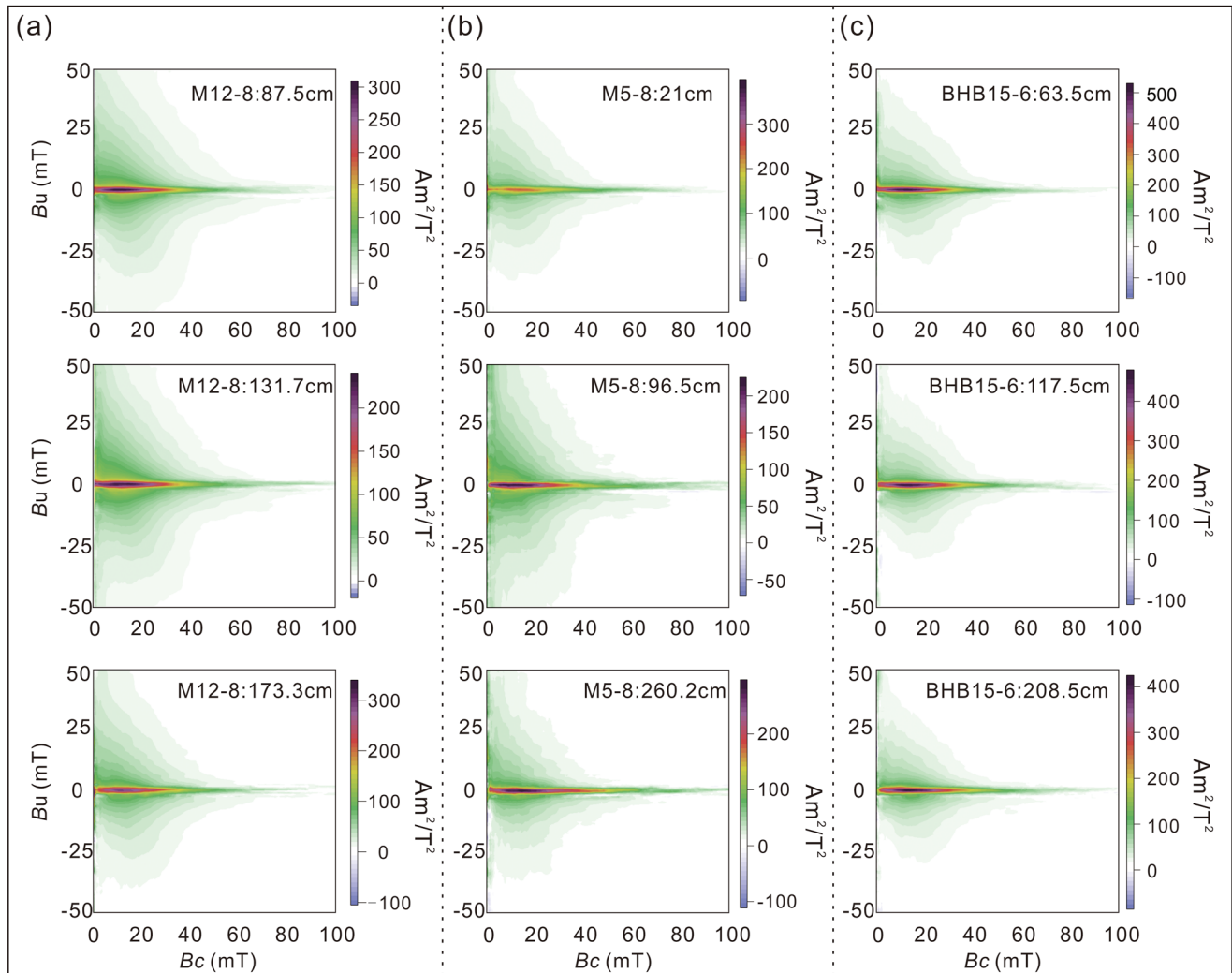


Figure 4. First order reversal curves diagrams for representative samples from cores (a) M12-8, (b) M5-8, and (c) BHB15-6.

to average out to a geocentric axial dipole (GAD). Although the Bohai Sea paleomagnetic records (<4 kyr) being shorter than required by the GAD hypothesis (>10 kyr), we choose this approach because it yields a reasonable agreement among the studied cores (Figure 5a) with the least number of assumptions required. The paleomagnetic stack curves (black curves, Figures 5a and 5c) were calculated using a bootstrap-running average method similar to that described by Cai et al. (2020). Specifically, we used the bootstrap technique with 1,000 times to calculate the 95% confidence interval of the data, and then applied a running average method with a time window of 30 years shifted by 30 years.

4. Reconstruction of Paleomagnetic Secular Variations

The PSV characteristics of the three studied cores are presented in Figure 5. RPI data between 30 Common Era (CE) to 820 CE (gray part of the M12-8 RPI curve, Figure 5c) for core M12-8 were excluded from further interpretations due to the inconsistency in RPI characteristics compared to the other two cores, potentially resulting from distinct environmental factors or other unknown mechanisms. The PSV features in core BHB15-6 are dissimilar from those of both cores M5-8 and M12-8 (Figure 5a), chiefly regarding the PSV declination. This discrepancy may be attributed to the significant difference in sedimentation rates at the studied areas, that is, ~50 cm/ka for BHB15-6 and ~130 cm/ka for other cores. The full vector PSV record for all studied cores, comprising ChRM direction (inclination and declination) and RPI, were stacked together and shown in Figures 5a–5c, with 95%

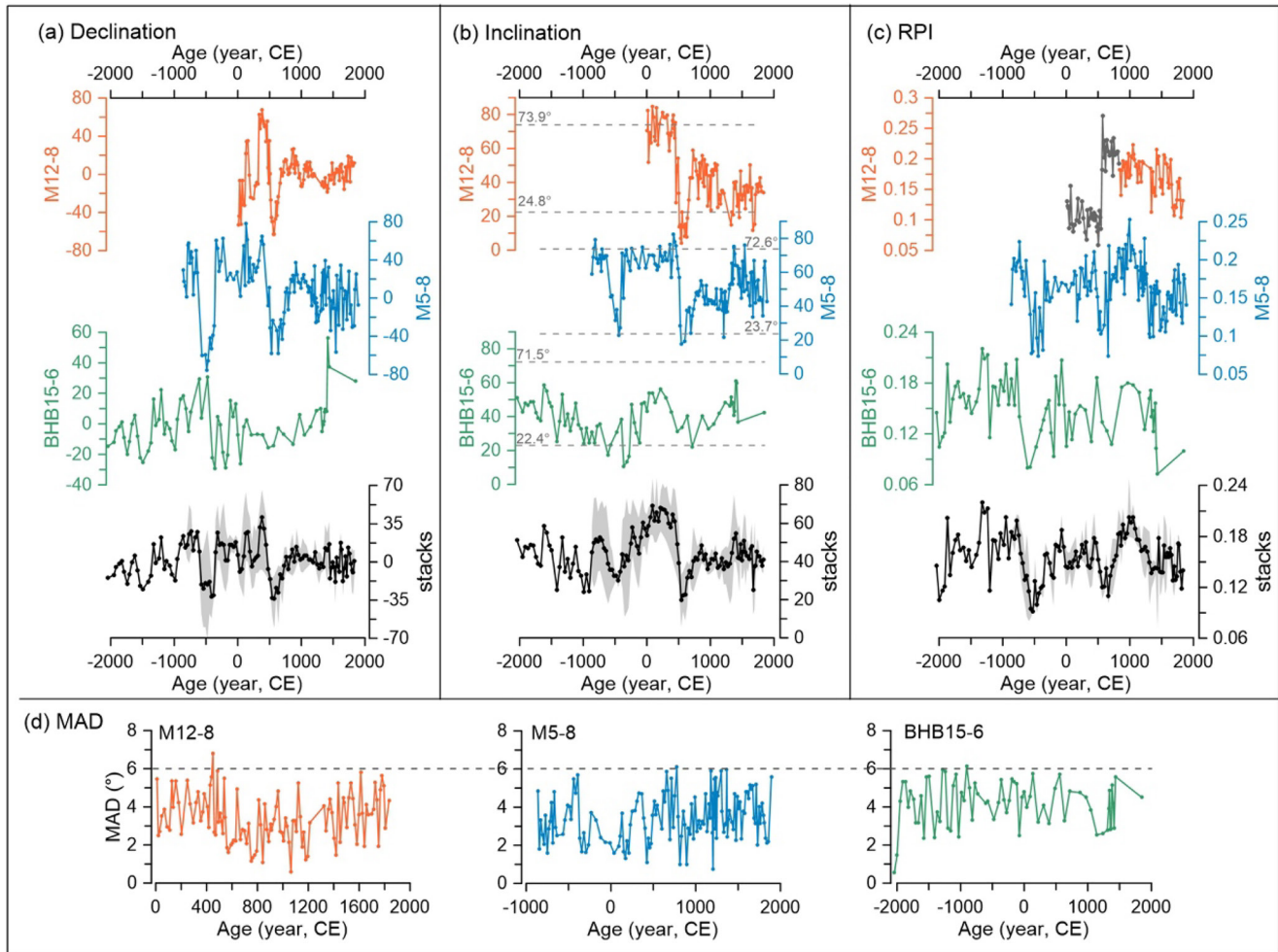


Figure 5. (a) Declination, (b) Inclination, and (c) relative paleointensity (RPI) records of three studied cores with their stack. The gray dash lines in (b) represents the 95% confidence levels at each core site and was calculated using the TK03.GAD model (Tauxe & Kent, 2004). The gray part of the M12-8 RPI curve is not used for calculating the stack. The 95% confidence of stack data is shown as light gray bars. (d) maximum angular deviation of characteristic remanent magnetization of three studied cores.

confidence intervals of means calculated by the bootstrap method. Only data from core BHB15-6, which includes sediments older than 800 before CE (BCE), were used to reconstruct the stack of that period.

As mentioned in Sections 3.2 and 3.3, our rock magnetic and demagnetization results have satisfied the conventional criteria for RPI studies (Tauxe, 1993). However, floc sizes, which are mainly affected by salinity, can partly control the acquisition of depositional remanent magnetization (Mitra & Tauxe, 2009; Tauxe et al., 2006), particularly in marginal seas (X. Yang et al., 2016). The salinity of water in the Bohai Sea is influenced by the water input from high-salinity ($\sim 33.5\text{‰}$) and high-temperature ($\sim 15^{\circ}\text{C}$, in winter) YSWC and river runoff (Lin et al., 2001; Ning et al., 2010). The sea surface temperature (SST) on the pathway of the YSWC can be a proxy of the YSWC strength (Y. He et al., 2014; Y. Zhang et al., 2019), while river runoff flowing into the Bohai Sea is governed by the intensity of East Asia Summer Monsoon (EASM). To assess the potential influence of flocculation on RPI variations, cross-wavelet transform analyses were performed to compare the evolution over the past 4 ka of the Bohai Sea RPI with the EASM and the SST records from the northern Yellow Sea (core 38002) (Y. Zhang et al., 2019; J. Zhang et al., 2020). The Bohai Sea RPI stack does not exhibit a significant correlation with either EASM or SST (Figure 6a). This lack of correlation is further supported by the cross wavelet transform (XWT) and squared wavelet coherence (WTC) analysis (Figures 6b–6e). The XWT and WTC results also show no evidence of a certain causal relationship between the Bohai Sea RPI stack and EASM or SST (Figures 6b–6e). Therefore, the salinity variations have a minor influence on RPI estimates, which further verifies the accuracy of the stacked Bohai Sea RPI record.

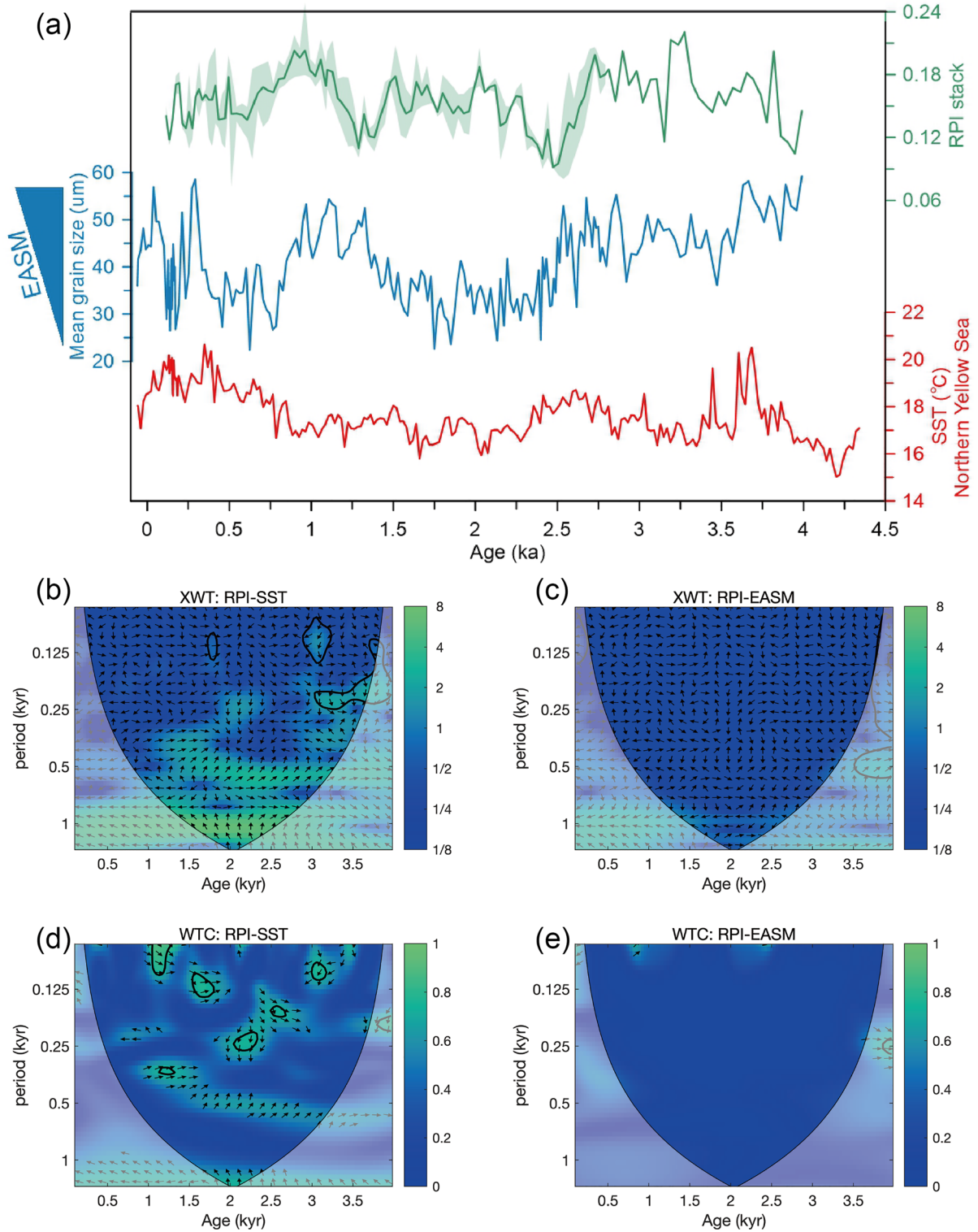


Figure 6. (a) The Bohai Sea RPI stack (green line), the East Asia Summer Monsoon (EASM) (blue line), and the sea surface temperature (SST) (red line) from the northern Yellow Sea (Y. Zhang et al., 2019; J. Zhang et al., 2020). (b) The cross wavelet transform (XWT) and (d) squared wavelet coherence (WTC) analysis between the Bohai Sea RPI stack SST. (c) The XWT and (e) WTC analysis between the Bohai Sea RPI stack EASM. The cross wavelet transforms between the Bohai Sea RPI stack and the EASM record. Phase arrows pointing right (left) indicate in-phase (anti-phase) for RPI and SST or EASM.

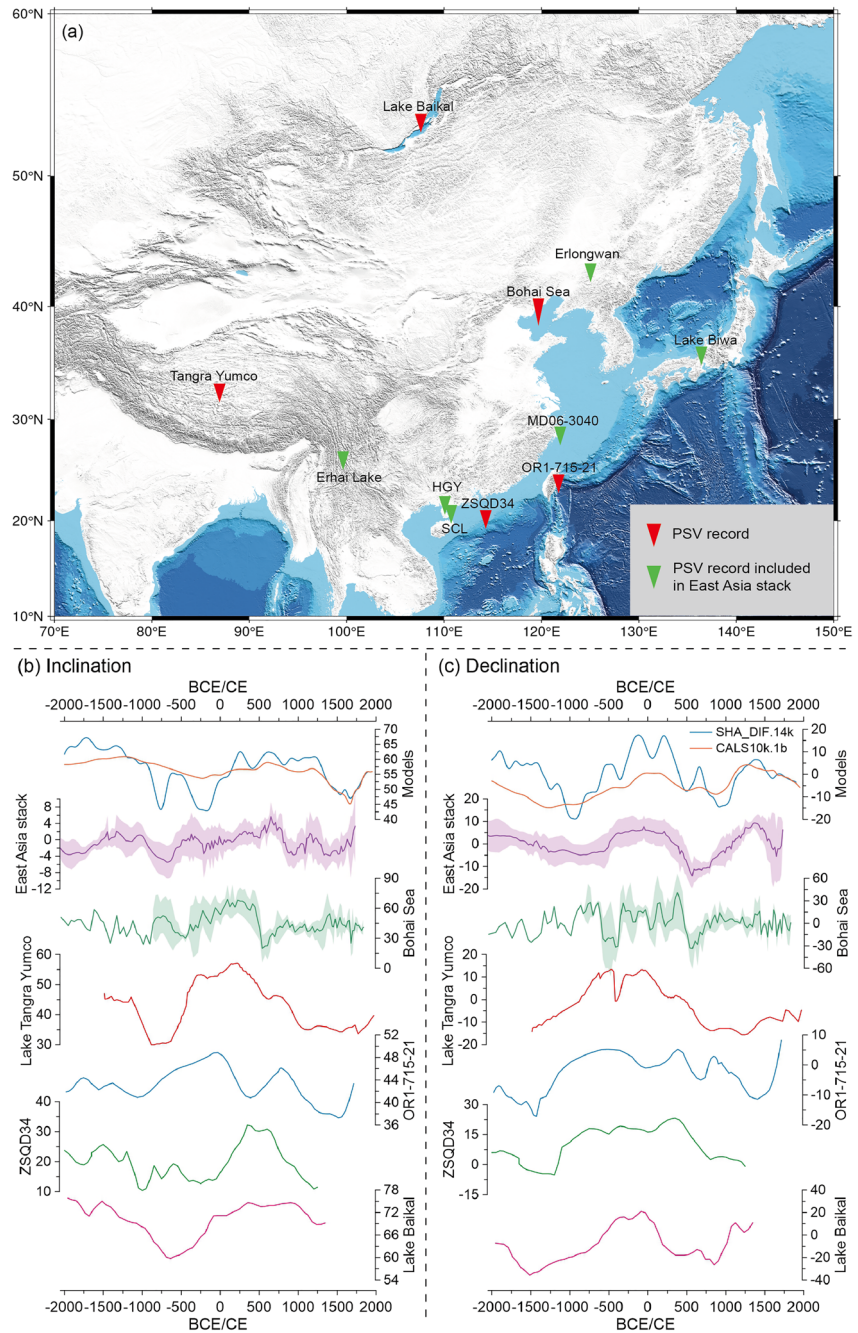


Figure 7. Comparison of the Bohai Sea paleomagnetic secular variation (PSV) records with East Asia stack (Zheng et al., 2014) and sediment PSV results from Lake Baikal (Peck et al., 1996), Lake Tangra Yumco (Haberzettl et al., 2015), core OR1-715-21 from offshore eastern Taiwan (Huang et al., 2014) and core ZSQD34 from the northern South China Sea (Yang et al., 2016) as well as model predictions (calculated at 39°N, 120°E) (Korte et al., 2011; Pavón-Carrasco et al., 2014). (a) PSV record position, (b) Inclination, (c) Declination.

5. Discussion

5.1. Variations in Paleomagnetic Directions of East Asia During the Late Holocene

A comparison between the Bohai Sea PSV (declination and inclination) stack and other regional PSV records over the late Holocene is presented in Figure 7, including records from Lake Baikal (Peck et al., 1996), the offshore eastern Taiwan core OR1-715-21 (Huang et al., 2014), Lake Tangra Yumco (Haberzettl et al., 2015) and

the northern South China Sea core ZSQD34 (X. Yang et al., 2016). The East Asia PSV stack (Zheng et al., 2014) and model-predicted PSV results at 39°N 120°E (Korte et al., 2011; Pavón-Carrasco et al., 2014) are also shown for comparison. The SHA.DIF.14k model is based solely on archeomagnetic and lava flow data (Pavón-Carrasco et al., 2014), while the CALS10k.1b model incorporates sediment data (Korte et al., 2011).

The Bohai Sea PSV record is quite similar to the East Asia PSV stack, characterized by relatively high inclination values between ~1500 and 1000 BCE and between ~500 BCE and 500 CE and low inclination values since ~700 CE (Figure 7b). The Bohai Sea PSV declination pattern also resembles the East Asia PSV stack since ~500 BCE (Figure 7c). Although the PSV variations in the Northern South China Sea (X. Yang et al., 2016), offshore eastern Taiwan (Huang et al., 2014), Lake Tangra Yumco (Haberzettl et al., 2015), and Lake Baikal (Peck et al., 1996) (Figure 7a) fluctuate less than the Bohai Sea PSV records, they all exhibit similar characteristics (Figures 7b and 7c). The Bohai Sea PSV record is, moreover, also consistent with the model-predicted PSV results at 39°N 120°E (Figures 7b and 7c). However, it should be noted that certain age offsets and inconsistencies have existed in all East Asia PSV records (Figures 7b and 7c), particularly between the mid- and low-latitude records such as the inclination features between the Bohai Sea stack and core OR1-715-21 (Figure 7b). These discrepancies may be caused by the lock-in process (Roberts & Winklhofer, 2004) and/or the non-dipole effect. The Siberian flux lobe, a persistent magnetic flux patch beneath Siberia (Korte & Holme, 2010), exerts a substantial influence on the geomagnetic field in East Asia and the subarctic Pacific Ocean (X. Yang et al., 2022; Zhong et al., 2020). This non-dipole component may contribute to an important effect on the inconsistent behavior of PSV between the mid- and low-latitudes in East Asia.

5.2. Late Holocene Paleointensity Variations in East Asia

The Bohai Sea RPI stack documents multi-decadal resolved geomagnetic field features during the late Holocene (since 2000 BCE). Our RPI stack is largely consistent with the model CALS10k.1b (Figure 8a, calculated at 39°N, 120°E; Korte et al., 2011) and the Chinese archeointensity reference curve (Figure 8b, Archint_China2, 105°E, 35°N; Cai et al., 2020) within age uncertainties. The Bohai Sea RPI stack, virtual axial dipole moment values in Archint_China2 and model CALS10k.1b are relatively higher over the intervals of ~1300 to 700 BCE and ~100 to 500 CE while inversely showing lower values from ~700 to 300 BCE, around 600 CE, and since 1200 CE (Figures 8a and 8b). However, the Bohai Sea RPI stack differs significantly from the low-latitude results of Tengchong Qinghai Lake (98.57°E, 25.13°N, Figure 8c; X. Yang et al., 2022) and core OR1-715-21 (121.29°E, 22.7°N, Figure 8d; Huang et al., 2014), particularly during the intervals of ~700 to 300 BCE and ~100 to 500 CE, where the low-latitude (Figures 8c and 8d) records are opposite to the mid-latitude records (Figures 8a and 8b).

The discrepancy in paleointensity behavior between the mid- (Figures 8a and 8b) and low-latitudes (<30°N, Figures 8c and 8d) East Asia, together with the behavior of paleomagnetic directions (Figures 7b and 7c), suggests the presence of the non-dipole effect in this region. Over the past 7,000 years, there have been two or three intense magnetic flux lobes beneath North America, Europe, and Siberia in the Northern Hemisphere (Blokhman et al., 1989; Korte & Holme, 2010). The expansion and intensification of these magnetic flux lobes would influence the behavior of regional magnetic fields (Gallet et al., 2009; X. Yang et al., 2022). Variations in the Bohai Sea RPI may reflect the varying activity of the Siberian surface lobe, which originates from the Siberian flux lobe located on the CMB (Blokhman & Gubbins, 1985; Livermore et al., 2020). As expected, periods of both strengthening and weakening of the magnetic field intensity in the Bohai Sea correlate well with the southeastward or northwestward movement of the Siberian surface lobe (Figure 9). Furthermore, the Siberian surface lobe and the north magnetic pole exhibited a coherent motion trend, with the southeastward movement and intensification of the Siberian surface lobe corresponding to a similar southeastward drift of the north magnetic pole, and vice versa (Figure 9).

The time-dependent position of the north magnetic pole position has been largely determined by the two competing magnetic flux lobes underneath Siberia and Canada (Livermore et al., 2020). The Siberian surface lobe is a spatial average over a region dominated by the large-scale lobe of intense magnetic flux beneath Siberia (Blokhman & Gubbins, 1985; Livermore et al., 2020). Although the geometric attenuation through the mantle means that the lobe between Earth's surface and CMB is not a simple mapping, the magnetic field at the Earth's surface is linearly related to the structure of the field on the CMB. The coherent variations observed in both the Siberian surface lobe and the north magnetic pole should reflect the changes in the magnetic flux lobe structure on the CMB (Figure 9). As demonstrated by the changes observed over the past few decades, the persistent strengthening of the Siberian flux lobe, coupled with the simultaneous weakening of the Canadian flux lobe, results in the strengthen of the Siberian

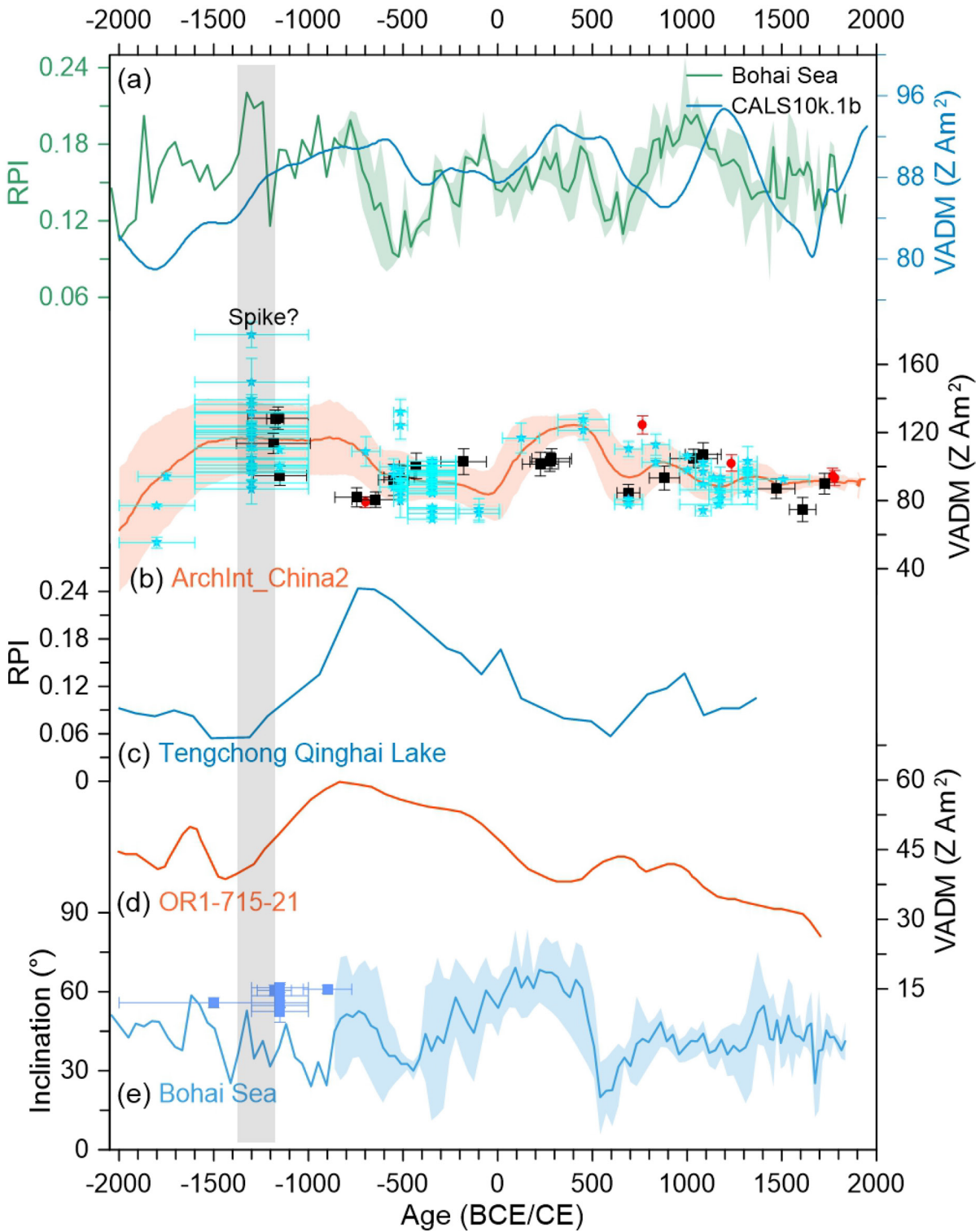


Figure 8. (a) Bohai Sea RPI stack with 95% confidence (green line), the blue line corresponds to the model paleointensity estimated by CALS10k.1b (Korte et al., 2011). (b) Chinese archeointensity reference curve-ArchInt_China2 (35°N, orange line; Cai et al., 2020). New publication of archeointensity data in China (Cai et al., 2014, 2017, 2020), Japan (Yu, 2012), and Korea (Hong et al., 2013) are respectively indicated by the cyan stars, red circles, and black squares. (c) RPI curve of Tengchong Qinghai Lake (without core top samples, 25.13°N; Yang et al., 2022). (d) Virtual axial dipole moment variations of core OR1-715-21 (22.7°N; Huang et al., 2014). (e) Bohai Sea inclination stack with 95% confidence (blue curve); the blue squares are archeomagnetic inclination results around the geomagnetic spike at 1300 BCE (Cai et al., 2016; Wei et al., 1984).

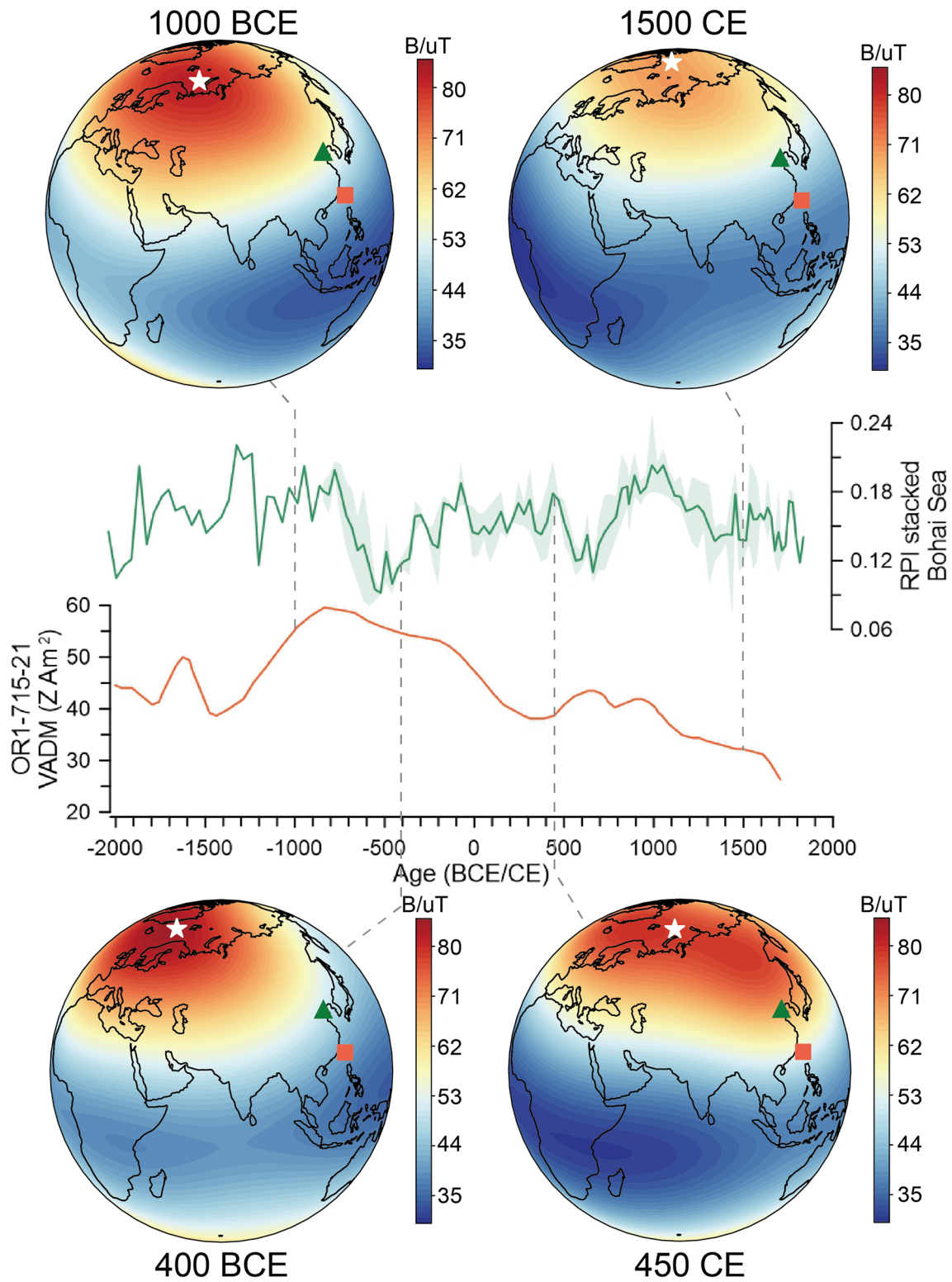


Figure 9. The Bohai Sea stacked RPI value correspondence to the variation of magnetic intensity lobe (calculated at the Earth's surface using the CALS10k.1b model, Korte et al., 2011). Green triangle: Bohai Sea; white star: north magnetic pole; orange square: core OR1-715-21 (Huang et al., 2014).

surface lobe and the northward shift of the magnetic pole toward the Siberian region (Livermore et al., 2020). Therefore, we propose that the corresponding variations in the Siberian surface lobe and the Bohai Sea RPI indicate the significant influence of the Siberian flux lobe on the magnetic field in the East Asian mid-latitude region. A higher magnetic field intensity corresponds to a relatively stronger Siberian flux lobe, and conversely, vice versa.

The RFPs, which are mainly concentrated in low-latitude areas, contribute to approximately 66% of the axial dipole decay (Metman et al., 2018) and exhibited a westward drift and migrating toward higher latitudes over the past 3 ka (Terra-Nova et al., 2015). Previous studies have indicated that these RFPs play a crucial role in governing the variations of the low geomagnetic anomaly across the equatorial latitudes, and consequently influence the magnetic field in Southeast and East Asia (Cai et al., 2021; F. He et al., 2021). The potential influence of RFPs on paleomagnetic behavior between mid- and low-latitudes in East Asia should also be considered. Figure 9 depicts a decrease in magnetic field intensity at low-latitude around 450 CE; however, simultaneously, the Siberian surface lobe extended southward. The reduced geomagnetic intensity in the low-latitude region during this period can be attributed to the northward movement and strengthening of the low geomagnetic anomaly (Figure 9) resulting from the presence of RFPs. This observation further suggests that RFPs likely exert a more pronounced effect in the low-latitude regions of East Asia.

In addition to the magnetic flux patch, the impact of the dipole moment on East Asia should be considered. Around 400 BCE, the lower magnetic field intensity in the Bohai Sea corresponds to the Siberian flux lobe (Figure 9), while the higher field intensity in core OR1-715-21 is likely related to the higher dipole moment (Figure S5 in Supporting Information S1). This higher dipole moment may have caused the relatively high magnetic field intensity in core OR1-715-21 around 400 BCE (Figure S5 in Supporting Information S1). Additionally, the relatively low magnetic field intensity in the Bohai Sea around 1500 CE may not only be due to the weakening of the Siberian flux lobe (Figure 9) but also be related to the decrease of the dipole moment (Figure S5 in Supporting Information S1).

In summary, we concluded that the paleointensity records from the middle (Figures 8a and 8b) and low latitudes (Figures 8c and 8d) are primarily affected by different non-dipole effects. The Siberian flux lobe dominates the evolution of geomagnetic field characteristics of mid- and high-latitude areas, while RFPs are more likely to affect the low-latitude area. The evolution of the Siberian flux lobe and RFPs can influence the regional surface geomagnetic field intensity (Hong et al., 2013), resulting in a geomagnetic field behavior disparity between mid- and low-latitude area of East Asia (X. Yang et al., 2022). Furthermore, the impact of the dipole moment cannot be ignored.

5.3. The Chinese Geomagnetic Spike

Apart from documenting the Siberian flux lobe evolution, the high-resolution Bohai Sea stacked RPI record also provides an opportunity to study the short-lived geomagnetic behavior, such as the geomagnetic spike (Cai et al., 2014). Our record shows an abrupt increase in RPI between 1233 and 1138 BCE (the gray region in Figure 8a), which could be correlated with the Chinese geomagnetic spike at around 1300 BCE (± 300 yr) (Cai et al., 2017). Moreover, the inclination of the Bohai Sea was relatively unchanged during this period and consistent with that in the archeomagnetic record (Figure 8e) (Cai et al., 2016; Wei et al., 1984).

Cai et al. (2017) proposed that the Chinese geomagnetic spike around 1300 BCE may be a precursor to the Levantine geomagnetic spike (~ 1000 BCE). Recent geomagnetic evolution models indicate that the Levantine geomagnetic spike is associated with the intense magnetic flux patch at the CMB beneath Western Asia (Davies & Constable, 2017; Korte & Constable, 2018; Osete et al., 2020), while the Chinese geomagnetic spike is linked with another magnetic flux patch (Korte & Constable, 2018). Furthermore, a large angular deviation was identified in the Levantine geomagnetic spike (Béguin et al., 2019; Ebert et al., 2021; Shaar et al., 2018), whereas there was no significant change in paleomagnetic directions in either the Bohai Sea or the archeomagnetic records (Figure 8e). These findings suggest that the Chinese and Levantine geomagnetic spikes might have originated from two separate magnetic flux patches, that is, beneath Eastern Asia (Chinese spike) and Western Asia (Levantine spike). Nevertheless, it should be noted that the anomalies in the direction and intensity of the geomagnetic field are not always synchronized, and the availability of archeomagnetic data is relatively limited. Further research with more robust data is required to investigate the origin of these spikes.

6. Conclusions

In this study, we reconstructed a stack of paleomagnetic records since 2000 BCE by using three marine sediment cores from the Bohai Sea. Magnetic minerals in the Bohai Sea sediments are dominated by fine-grained magnetite

with slight grain size change. The Bohai Sea paleomagnetic record differs from the East Asia low-latitude results and is mainly affected by the migration of the Siberian flux lobe. The Bohai Sea RPI stack indicates that the Chinese geomagnetic spike occurred between 1233 and 1138 BCE. The discrepancy in inclination between the Chinese and Levantine geomagnetic spikes, coupled with prior model findings, indicates that these spikes might originated from two distinct magnetic flux patches. However, further robust data are necessary for a comprehensive investigation of the origin of these spikes.

Data Availability Statement

See H. Li et al. (2023) <https://zenodo.org/records/10045893> for the data acquired during this study.

Acknowledgments

The authors would like to express their gratitude to Prof. Jiabo Liu for his valuable contributions in improving the manuscript. The authors express their gratitude to Professor F. Javier Pavón-Carrasco and the anonymous reviewer for their insightful input which helped us to improve the manuscript. This work was supported by the National Natural Science Foundation of China (92158208, 42074071, 41874078, 42104068, 42204080), Shenzhen Science and Technology Program (KQTD20170810111725321, KCXFZ20211020174803005), Science and Technology Innovation Committee of Shenzhen Municipality (ZDSYS201802081843490), Technology and Innovation Commission of Shenzhen Municipality (20200925154739001), Southern University of Science and Technology (Y01316111), Key Special Project for Introduced Talents Team of Southern Marine Science and Engineering Guangdong Laboratory (Guangzhou) (GML2019ZD0210), the opening foundation (SSKP202101) of the Shanghai Sheshan National Geophysical Observatory (Shanghai, China).

References

- Alken, P., Thébault, E., Beggan, C. D., Amit, H., Aubert, J., Baerenzung, J., et al. (2021). International geomagnetic reference field: The thirteenth generation. *Earth Planets and Space*, 73(1), 49. <https://doi.org/10.1186/s40623-020-01288-x>
- Amit, H., Aubert, J., & Hulot, G. (2010). Stationary, oscillating or drifting mantle-driven geomagnetic flux patches? *Journal of Geophysical Research*, 115(B7), B07108. <https://doi.org/10.1029/2009JB006542>
- Amit, H., Korte, M., Aubert, J., Constable, C., & Hulot, G. (2011). The time-dependence of intense archeomagnetic flux patches. *Journal of Geophysical Research*, 116(B12), B12106. <https://doi.org/10.1029/2011JB008538>
- Béguin, A., Filippidi, A., de Lange, G. J., & de Groot, L. V. (2019). The evolution of the Levantine Iron age geomagnetic anomaly captured in mediterranean sediments. *Earth and Planetary Science Letters*, 511, 55–66. <https://doi.org/10.1016/j.epsl.2019.01.021>
- Bloxham, J., & Gubbins, D. (1985). The secular variation of Earth's magnetic field. *Nature*, 317(6040), 777–781. <https://doi.org/10.1038/317777a0>
- Bloxham, J., Gubbins, D., Jackson, A., & McKenzie, D. P. (1989). Geomagnetic secular variation. *Philosophical Transactions of the Royal Society of London. Series A, Mathematical and Physical Sciences*, 329(1606), 415–502. <https://doi.org/10.1098/rsta.1989.0087>
- Buffett, B. A. (2000). Earth's core and the geodynamo. *Science*, 288(5473), 2007–2012. <https://doi.org/10.1126/science.288.5473.2007>
- Cai, S., Doctor, R., Tauxe, L., Hendrickson, M., Hua, Q., Leroy, S., & Phon, K. (2021). Archaeomagnetic results from Cambodia in Southeast Asia: Evidence for possible low-latitude flux expulsion. *Proceedings of the National Academy of Sciences*, 118(11), e2022490118. <https://doi.org/10.1073/pnas.2022490118>
- Cai, S., Jin, G., Tauxe, L., Deng, C., Qin, H., Pan, Y., & Zhu, R. (2017). Archaeointensity results spanning the past 6 kiloyears from eastern China and implications for extreme behaviors of the geomagnetic field. *Proceedings of the National Academy of Sciences*, 114(1), 39–44. <https://doi.org/10.1073/pnas.1616976114>
- Cai, S., Tauxe, L., Deng, C., Pan, Y., Jin, G., Zheng, J., et al. (2014). Geomagnetic intensity variations for the past 8 kyr: New archaeointensity results from Eastern China. *Earth and Planetary Science Letters*, 392, 217–229. <https://doi.org/10.1016/j.epsl.2014.02.030>
- Cai, S., Tauxe, L., Deng, C., Qin, H., Pan, Y., Jin, G., et al. (2016). New archaeomagnetic direction results from China and their constraints on palaeosecular variation of the geomagnetic field in Eastern Asia. *Geophysical Journal International*, 207(2), 1332–1342. <https://doi.org/10.1093/gji/ggw351>
- Cai, S., Tauxe, L., Wang, W., Deng, C., Pan, Y., Yang, L., & Qin, H. (2020). High-Fidelity archeointensity results for the late neolithic period from Central China. *Geophysical Research Letters*, 47(10), 1–11. <https://doi.org/10.1029/2020GL087625>
- Caricchi, C., Campuzano, S. A., Sagnotti, L., Macri, P., & Lucchi, R. G. (2022). Reconstruction of the Virtual Geomagnetic Pole (VGP) path at high latitude for the last 22 kyr: The role of radial field flux patches as VGP attractor. *Earth and Planetary Science Letters*, 595, 117762. <https://doi.org/10.1016/j.epsl.2022.117762>
- Carlut, J., & Courtillot, V. (1998). How complex is the time-averaged geomagnetic field over the past 5 Myr? *Geophysical Journal International*, 134(2), 527–544. <https://doi.org/10.1046/j.1365-246X.1998.00577.x>
- Chen, L., Luan, Z., Zhen, T., Xu, W., & Dong, T. (1982). Mineral assemblages and their distribution patterns in the sediments of the Gulf of Bohai Sea. *Chinese Journal of Oceanology and Limnology*, 1(1), 82–103. <https://doi.org/10.1007/BF02852892>
- Constable, C., Korte, M., & Panovska, S. (2016). Persistent high paleosecular variation activity in southern hemisphere for at least 10 000 years. *Earth and Planetary Science Letters*, 453, 78–86. <https://doi.org/10.1016/j.epsl.2016.08.015>
- Davies, C., & Constable, C. (2017). Geomagnetic spikes on the core-mantle boundary. *Nature Communications*, 8(May), 1–11. <https://doi.org/10.1038/ncomms15593>
- Dunlop, D. J., & Özdemir, Ö. (1997). *Rock magnetism: Fundamentals and frontiers*. Cambridge University Press.
- Ebert, Y., Shaar, R., & Stein, M. (2021). Decadal geomagnetic secular variations from greigite bearing dead Sea sediments. *Geochemistry, Geophysics, Geosystems*, 22(4), 1–15. <https://doi.org/10.1029/2021GC009665>
- Egli, R., Chen, A. P., Winklhofer, M., Kodama, K. P., & Horng, C.-S. (2010). Detection of noninteracting single domain particles using first-order reversal curve diagrams. *Geochemistry, Geophysics, Geosystems*, 11(1), 334. <https://doi.org/10.1029/2009gc002916>
- Finlay, C. C., Kloss, C., Olsen, N., Hammer, M. D., Clausen, L. T., Grayver, A., & Kuvshinov, A. (2020). The CHAOS—7 geomagnetic field model and observed changes in the South Atlantic Anomaly. *Earth Planets and Space*, 72(1), 156. <https://doi.org/10.1186/s40623-020-01252-9>
- Gallet, Y., Hulot, G., Chulliat, A., & Genevey, A. (2009). Geomagnetic field hemispheric asymmetry and archeomagnetic jerks. *Earth and Planetary Science Letters*, 284(1–2), 179–186. <https://doi.org/10.1016/j.epsl.2009.04.028>
- Haberzettl, T., Henkel, K., Kasper, T., Ahlborn, M., Su, Y., Wang, J., et al. (2015). Independently dated paleomagnetic secular variation records from the Tibetan Plateau. *Earth and Planetary Science Letters*, 416, 98–108. <https://doi.org/10.1016/j.epsl.2015.02.007>
- Harrison, R. J., & Feinberg, J. M. (2008). FORCinel: An improved algorithm for calculating first-order reversal curve distributions using locally weighted regression smoothing. *Geochemistry, Geophysics, Geosystems*, 9(5), Q05016. <https://doi.org/10.1029/2008GC001987>
- He, F., Wei, Y., Maffei, S., Livermore, P. W., Davies, C. J., Mound, J., et al. (2021). Equatorial auroral records reveal dynamics of the paleo-West Pacific geomagnetic anomaly. *Proceedings of the National Academy of Sciences of the United States of America*, 118(20), e2026080118. <https://doi.org/10.1073/pnas.2026080118>
- He, Y., Zhou, X., Liu, Y., Yang, W., Kong, D., Sun, L., & Liu, Z. (2014). Weakened Yellow Sea Warm current over the last 2-3 centuries. *Quaternary International*, 349, 252–256. <https://doi.org/10.1016/j.quaint.2013.09.039>

- Heaton, T. J., Köhler, P., Butzin, M., Bard, E., Reimer, R. W., Austin, W. E. N., et al. (2020). Marine20—The marine radiocarbon age calibration curve (0–55,000 cal BP). *Radiocarbon*, 62(4), 779–820. <https://doi.org/10.1017/RDC.2020.68>
- Hong, H., Yu, Y., Lee, C. H., Kim, R. H., Park, J., Doh, S.-J., et al. (2013). Globally strong geomagnetic field intensity circa 3000 years ago. *Earth and Planetary Science Letters*, 383, 142–152. <https://doi.org/10.1016/j.epsl.2013.09.043>
- Hrouda, F., & Kahan, S. (1991). The magnetic fabric relationship between sedimentary and basement nappes in the High Tatra Mountains, N. Slovakia. *Journal of Structural Geology*, 13(4), 431–442. [https://doi.org/10.1016/0191-8141\(91\)90016-C](https://doi.org/10.1016/0191-8141(91)90016-C)
- Huang, Y.-S., Lee, T.-Q., & Wei, K.-Y. (2014). Dominant dipole effect embedded in paleomagnetic secular variation in Taiwan region over the past 7500 years. *Physics of the Earth and Planetary Interiors*, 234, 14–22. <https://doi.org/10.1016/j.pepi.2014.06.011>
- Johnson, C. L., & Constable, C. G. (1995). The time-averaged geomagnetic field as recorded by lava flows over the past 5 Myr. *Geophysical Journal International*, 122(2), 489–519. <https://doi.org/10.1111/j.1365-246X.1995.tb07010.x>
- Kelly, P., & Gubbins, D. (1997). The geomagnetic field over the past 5 million years. *Geophysical Journal International*, 128(2), 315–330. <https://doi.org/10.1111/j.1365-246X.1997.tb01557.x>
- Khokhlov, A., Hulot, G., & Bouligand, C. (2006). Testing statistical palaeomagnetic field models against directional data affected by measurement errors. *Geophysical Journal International*, 167(2), 635–648. <https://doi.org/10.1111/j.1365-246X.2006.03133.x>
- King, J., Banerjee, S. K., Marvin, J., & Özdemir, Ö. (1982). A comparison of different magnetic methods for determining the relative grain size of magnetite in natural materials: Some results from lake sediments. *Earth and Planetary Science Letters*, 59(2), 404–419. [https://doi.org/10.1016/0012-821X\(82\)90142-X](https://doi.org/10.1016/0012-821X(82)90142-X)
- King, J. W., Banerjee, S. K., & Marvin, J. (1983). A new rock-magnetic approach to selecting sediments for geomagnetic paleointensity studies: Application to paleointensity for the last 4000 years. *Journal of Geophysical Research*, 88(B7), 5911–5921. <https://doi.org/10.1029/JB088iB07p05911>
- Kirschvink, J. L. (1980). The least-squares line and plane and the analysis of palaeomagnetic data. *Geophysical Journal of the Royal Astronomical Society*, 62(3), 699–718. <https://doi.org/10.1111/j.1365-246X.1980.tb02601.x>
- Korte, M., Constable, C., Donadini, F., & Holme, R. (2011). Reconstructing the Holocene geomagnetic field. *Earth and Planetary Science Letters*, 312(3–4), 497–505. <https://doi.org/10.1016/j.epsl.2011.10.031>
- Korte, M., & Constable, C. G. (2018). Archeomagnetic intensity spikes: Global or regional geomagnetic field features? *Frontiers in Earth Science*, 6(March), 1–15. <https://doi.org/10.3389/feart.2018.00017>
- Korte, M., & Holme, R. (2010). On the persistence of geomagnetic flux lobes in global Holocene field models. *Physics of the Earth and Planetary Interiors*, 182(3–4), 179–186. <https://doi.org/10.1016/j.pepi.2010.08.006>
- Lascu, I., Einsle, J. F., Ball, M. R., & Harrison, R. J. (2018). The vortex state in geologic materials: A micromagnetic perspective. *Journal of Geophysical Research: Solid Earth*, 123(9), 7285–7304. <https://doi.org/10.1029/2018JB015909>
- Li, H., Tang, J., Gai, C., Zhang, W., Humbert, F., Ni, Y., et al. (2023). Persistent influence of non-dipole geomagnetic field on East Asia over the past 4,000 years [Dataset]. Zenodo. <https://doi.org/10.5281/zenodo.10045893>
- Li, M., Zhu, S., Ouyang, T., Tang, J., & He, C. (2020). Magnetic fingerprints of surface sediment in the Bohai Sea, China. *Marine Geology*, 427(May), 106226. <https://doi.org/10.1016/j.margeo.2020.106226>
- Lin, C., Su, J., Xu, B., & Tang, Q. (2001). Long-term variations of temperature and salinity of the Bohai Sea and their influence on its ecosystem. *Progress in Oceanography*, 49(1–4), 7–19. [https://doi.org/10.1016/S0079-6611\(01\)00013-1](https://doi.org/10.1016/S0079-6611(01)00013-1)
- Liu, J., Nowaczyk, N., Frank, U., & Arz, H. (2019). Geomagnetic paleosecular variation record spanning from 40 to 20 ka—Implications for the Mono Lake excursion from Black Sea sediments. *Earth and Planetary Science Letters*, 509, 114–124. <https://doi.org/10.1016/j.epsl.2018.12.029>
- Livermore, P. W., Finlay, C. C., & Bayliff, M. (2020). Recent north magnetic pole acceleration towards Siberia caused by flux lobe elongation. *Nature Geoscience*, 13(5), 387–391. <https://doi.org/10.1038/s41561-020-0570-9>
- Lougheed, B. C., & Obrochta, S. P. (2019). A rapid, deterministic age-depth modeling routine for geological sequences with inherent depth uncertainty. *Paleoceanography and Paleoclimatology*, 34(1), 122–133. <https://doi.org/10.1029/2018PA003457>
- Metman, M. C., Livermore, P. W., & Mound, J. E. (2018). The reversed and normal flux contributions to axial dipole decay for 1880–2015. *Physics of the Earth and Planetary Interiors*, 276, 106–117. <https://doi.org/10.1016/j.pepi.2017.06.007>
- Mitra, R., & Tauxe, L. (2009). Full vector model for magnetization in sediments. *Earth and Planetary Science Letters*, 286(3–4), 535–545. <https://doi.org/10.1016/j.epsl.2009.07.019>
- Ning, X., Lin, C., Su, J., Liu, C., Hao, Q., Le, F., & Tang, Q. (2010). Long-term environmental changes and the responses of the ecosystems in the Bohai Sea during 1960–1996. *Deep-Sea Research Part II Topical Studies in Oceanography*, 57(11–12), 1079–1091. <https://doi.org/10.1016/j.dsr2.2010.02.010>
- Osete, M. L., Molina-Cardín, A., Campuzano, S. A., Aguilera-Arzo, G., Barrachina-Ibañez, A., Falomir-Granell, F., et al. (2020). Two archaeomagnetic intensity maxima and rapid directional variation rates during the Early Iron Age observed at Iberian coordinates. Implications on the evolution of the Levantine Iron Age Anomaly. *Earth and Planetary Science Letters*, 533, 116047. <https://doi.org/10.1016/j.epsl.2019.116047>
- Pavón-Carrasco, F. J., Osete, M. L., Torta, J. M., & de Santis, A. (2014). A geomagnetic field model for the Holocene based on archaeomagnetic and lava flow data. *Earth and Planetary Science Letters*, 388, 98–109. <https://doi.org/10.1016/j.epsl.2013.11.046>
- Peck, J. A., King, J. W., Colman, S. M., & Kravchinsky, V. A. (1996). An 84-kyr paleomagnetic record from the sediments of Lake Baikal, Siberia. *Journal of Geophysical Research B: Solid Earth*, 101(5), 11365–11385. <https://doi.org/10.1029/96jb00328>
- Pike, C. R., Roberts, A. P., & Verosub, K. L. (1999). Characterizing interactions in fine magnetic particle systems using first order reversal curves. *Journal of Applied Physics*, 85(9), 6660–6667. <https://doi.org/10.1063/1.370176>
- Qiao, L., Bao, X., & Wu, D. (2008). The observed currents in summer in the Bohai Sea. *Chinese Journal of Oceanology and Limnology*, 26(2), 130–136. <https://doi.org/10.1007/s00343-008-0130-4>
- Roberts, A. P., Almeida, T. P., Church, N. S., Harrison, R. J., Heslop, D., Li, Y., et al. (2017). Resolving the origin of pseudo-single domain magnetic behavior. *Journal of Geophysical Research: Solid Earth*, 122(12), 9534–9558. <https://doi.org/10.1002/2017JB014860>
- Roberts, A. P., & Winklhofer, M. (2004). Why are geomagnetic excursions not always recorded in sediments? Constraints from post-depositional remanent magnetization lock-in modelling. *Earth and Planetary Science Letters*, 227(3–4), 345–359. <https://doi.org/10.1016/j.epsl.2004.07.040>
- Shaar, R., Hassul, E., Raphael, K., Ebert, Y., Segal, Y., Eden, I., et al. (2018). The first catalog of archaeomagnetic directions from Israel with 4,000 Years of geomagnetic secular variations. *Frontiers in Earth Science*, 6(October). <https://doi.org/10.3389/feart.2018.00164>
- Southon, J., Kashgarian, M., Fontugne, M., Metivier, B., & Yim, W. W. S. (2002). Marine reservoir corrections for the Indian Ocean and Southeast Asia. In *Radiocarbon* (Vol. 44, pp. 167–180). <https://doi.org/10.1017/S0033822200064778>
- Stuiver, M., & Reimer, P. J. (1993). Extended 14 C data base and revised CALIB 3.0 14 C age calibration Program. *Radiocarbon*, 35(1), 215–230. <https://doi.org/10.1017/S0033822200013904>

- Tarduno, J. A., Watkeys, M. K., Huffman, T. N., Cottrell, R. D., Blackman, E. G., Wendt, A., et al. (2015). Antiquity of the South Atlantic Anomaly and evidence for top-down control on the geodynamo. *Nature Communications*, *6*(1), 7865. <https://doi.org/10.1038/ncomms8865>
- Tauxe, L. (1993). Sedimentary records of relative paleointensity of the geomagnetic field: Theory and practice. *Reviews of Geophysics*, *31*(3), 319–354. <https://doi.org/10.1029/93RG01771>
- Tauxe, L., & Kent, D. V. (2004). A simplified statistical model for the geomagnetic field and the detection of shallow bias in paleomagnetic inclinations: Was the ancient magnetic field dipolar? In *Geophysical monograph series* (Vol. 145, pp. 101–115). <https://doi.org/10.1029/145GM08>
- Tauxe, L., Steindorf, J. L., & Harris, A. (2006). Depositional remanent magnetization: Toward an improved theoretical and experimental foundation. *Earth and Planetary Science Letters*, *244*(3–4), 515–529. <https://doi.org/10.1016/j.epsl.2006.02.003>
- Terra-Nova, F., Amit, H., Hartmann, G. A., & Trindade, R. I. F. (2015). The time dependence of reversed archeomagnetic flux patches. *Journal of Geophysical Research: Solid Earth*, *120*(2), 691–704. <https://doi.org/10.1002/2014JB011742>
- Wei, Q., Li, D., Cao, G., Zhang, W., & Wang, S. (1984). The wandering path of virtual geomagnetic pole during the last 6000 years. *Advances in Geophysical Research*, *27*(6), 562–572.
- Yang, T., Zhao, X., Petronotis, K., Dekkers, M. J., & Xu, H. (2019). Anisotropy of magnetic susceptibility (AMS) of sediments from holes U1480E and U1480H, IODP expedition 362: Sedimentary or artificial origin and implications for paleomagnetic studies. *Geochemistry, Geophysics, Geosystems*, *20*(11), 5192–5215. <https://doi.org/10.1029/2019GC008721>
- Yang, X., Liu, Q., Yu, K., Huang, W., Zhu, L., Zhang, H., et al. (2016). Paleosecular variations of the geomagnetic field during the Holocene from eastern Asia. *Physics of the Earth and Planetary Interiors*, *254*, 25–36. <https://doi.org/10.1016/j.pepi.2016.03.004>
- Yang, X., Zhang, T., Zhang, E., Toney, J., Zhou, Q., & Xie, Y. (2022). Paleosecular variations during the last glacial period from Tengchong Qinghai Lake, Yunnan province, China. *Journal of Geophysical Research: Solid Earth*, *127*(3), e2020JB020593. <https://doi.org/10.1029/2021JB023459>
- Yao, Z., Shi, X., Liu, Q., Liu, Y., Larrasoana, J. C., Liu, J., et al. (2014). Paleomagnetic and astronomical dating of sediment core BH08 from the Bohai Sea, China: Implications for glacial-interglacial sedimentation. *Palaeogeography, Palaeoclimatology, Palaeoecology*, *393*, 90–101. <https://doi.org/10.1016/j.palaeo.2013.11.012>
- Yu, Y. (2012). High-fidelity paleointensity determination from historic volcanoes in Japan. *Journal of Geophysical Research*, *117*(B8), B08101. <https://doi.org/10.1029/2012JB009368>
- Zhang, J., Zhou, X., Jiang, S., Tu, L., & Liu, X. (2020). Monsoon precipitation, economy and wars in ancient China. *Frontiers in Earth Science*, *8*(July), 1–10. <https://doi.org/10.3389/feart.2020.00317>
- Zhang, Y., Zhou, X., He, Y., Jiang, Y., Liu, Y., Xie, Z., et al. (2019). Persistent intensification of the Kuroshio Current during late Holocene cool intervals. *Earth and Planetary Science Letters*, *506*, 15–22. <https://doi.org/10.1016/j.epsl.2018.10.018>
- Zheng, Y., Zheng, H., Deng, C., & Liu, Q. (2014). Holocene paleomagnetic secular variation from East China Sea and a PSV stack of East Asia. *Physics of the Earth and Planetary Interiors*, *236*, 69–78. <https://doi.org/10.1016/j.pepi.2014.07.001>
- Zhong, Y., Liu, Y., Yang, X., Zhang, J., Liu, J., Bosin, A., et al. (2020). Do non-dipole geomagnetic field behaviors persistently exist in the subarctic Pacific Ocean over the past 140 ka? *Science Bulletin*, *65*(18), 1505–1507. <https://doi.org/10.1016/j.scib.2020.05.016>

References From the Supporting Information

- Tauxe, L., Shaar, R., Jonestrask, L., Swanson-Hysell, N. L., Minnett, R., Koppers, A. A. P., et al. (2016). PmagPy: Software package for paleomagnetic data analysis and a bridge to the magnetics information consortium (MagIC) database. *Geochemistry, Geophysics, Geosystems*, *17*(6), 2450–2463. <https://doi.org/10.1002/2016GC006307>